ACTA ACUSTICA UNITED WITH ACUSTICA
Vol. 88 (2002) 252 – 261

Reverberation Times Obtained Using a Numerical Model Versus Those Given by Simplified Formulas and Measurements

J. António, L. Godinho, A. Tadeu
Civil Engineering Department, Faculty of Sciences and Technology, University of Coimbra, Portugal

Summary
This paper describes a set of analytical solutions used to evaluate the pressure response inside an empty parallelepiped closed space subjected to a harmonic point source. The model allows different absorption coefficients to be defined for the various walls, as well as frequency variation. The computations are first performed in the frequency domain and Inverse Fourier Transforms are subsequently applied to obtain impulse responses. The time-aliasing phenomenon is avoided by using complex frequencies to attenuate the response at the end of the time frame. This effect is later taken into account by re-scaling the response in the time domain. The model developed was applied to different scenarios for which reverberation times were computed using the Schroeder approach. Pulses with varying characteristic frequencies were modeled so that the influence of the excitation frequency on the reverberation times could be studied. These results were then compared with those provided by the simplified models of Sabine, Eyring, Millington, Fitzroy and Arau-Puchades. Experimental measurements in situ were also compared with those provided by the numerical model.

PACS no. 43.55.Br

1. Introduction

The acoustic design of closed spaces requires the study of pressure wave propagation in a frequency domain that ranges from low frequencies to frequencies up to 20.0 kHz. The propagation inside an enclosed space depends on the frequency of excitation, the material properties of the wall surfaces such as absorption and diffusion factors, air absorption, and indoor environmental conditions such as the temperature, air pressure and humidity. Given the complexity of the problem and the amount of computational effort required, different numerical schemes for predicting the sound propagation inside an enclosed room have been proposed and developed over the years.

Ray tracing and image model techniques are frequently used in an attempt to overcome the computational cost limitations, and they are currently applied to the study of acoustic wave propagation in closed and open spaces [1, 2, 3, 4, 5, 6].

With the ray tracing technique, generally applied in the high frequency domain, a number of finite rays are followed between the source and the receivers. Although the response can be computed in a reasonable time, it is not possible to ensure that all the rays contributing to an accurate response are taken into account, which introduces an element of uncertainty into the results [7]. Modeling diffuse reflection effects with sufficient detail, using room acoustics prediction methods based on geometrical acoustics, has been found to be difficult. Hodgson [8] used a ray tracing model that takes diffuse surface reflection into account according to Lambert's law [9] to predict the sound field in empty rooms. Predicted and measured sound decays have been compared [10]. It was concluded that the effects of diffuse surface reflection are negligible in small or proportionate rooms, while in large disproportionate rooms they can be considerable. Dalenbäck later proposed an algorithm based on approximate cone tracing, handling diffuse reflection by splitting up the cones incident on diffusing surfaces [11].

The image model technique employs virtual sources (image sources) to compute the acoustic field. These sources are placed so that they can simulate the reflections caused by the reflecting walls. This technique is reliable, but the computations involving models with complex geometry can become very complicated, and entail high computational costs. In general all surfaces are assumed to give only specular reflections.

This technique has already been applied in the time domain by several authors, including Gibbs and Jones [12] and Allen and Berkley [2]. Allen and Berkley computed the response between two points in a small rectangular room, convolved with any type of input signal, such as the sound of speech. The calculated impulse response is built up as a "histogram" of image sources received at different time delays. Borish subsequently extended the use of the

Received 22 February 2001,
accepted 26 November 2001.

image model technique to more complex geometries, such as a polyhedron with any number of sides [13].

Different computer codes have been proposed to predict sound levels and reverberation times based on both ray tracing and image source techniques [14, 15, 16]. Dance *et al.* [17] used different computer approaches and classical simplified formulae to study the accuracy of reverberation time predictions in a room with an uneven distribution of surface absorption. Their computations have only been performed for 1.0 kHz. It was found that the Eyring and Millington classical formulae could not accurately predict the reverberation times in a room where different absorptive surface properties were ascribed to the walls.

Several comparisons of room simulation software have been performed, as reported by Bork [18]. This work confirms that computer simulation is strongly dependent on the input data and the sensitivity of the operator to the absorption data of the surfaces, as well as the diffusivity properties of the wall material. The deviations occurred in the low frequency calculations, where the diffraction effects are important, but disregarded in the geometrical calculations. It is suggested that other methods, such as the Boundary Elements Method, could be used to compute the results at frequencies below 100 Hz [19].

Well-established numerical techniques, such as the finite element method (FEM) and finite difference method, have not been widely used to compute the propagation of sound, because of the high computation cost entailed. They have failed because the domain being analysed has to be fully discretized, and very fine meshes are needed to solve excitations at high frequencies.

Other methods, such as the Boundary Element Method (BEM), are more efficient in terms of computer cost as they only require the discretization of the boundaries [20]. But they nevertheless involve a large computational effort, particularly for very high frequencies. The solution becomes simpler in two-and-a-half-dimensional spaces (or 2-1/2-D for short), where the medium is two-dimensional (2D), but the dynamic source is three-dimensional (3D), such as a point source. The results are arrived at by using a spatial Fourier transform in the direction in which the geometry does not vary, which allows the solution to be obtained as a summation of 2D responses for a continuous variation of spatial wavenumbers [21, 22]. In the case of a frequency domain formulation, an additional Fourier transformation in the time domain is required.

The Fourier transformations are achieved by discrete summations over frequencies, which is the mathematical equivalent of adding periodic sources at temporal intervals $TD = 2\pi/\Delta\omega$, with $\Delta\omega$ being the frequency steps. In order to avoid contamination of the response by the periodic sources, known as time-aliasing effects, the acoustic signals are computed using complex frequencies ($\omega_c = \omega - \mathrm{i}\eta$). The use of complex frequencies would not be necessary if small frequency increments, $\Delta\omega$, were used to allow the full dynamic response to develop within the time window. The influence of the complex part (η) of the frequency is removed in the time domain, re-scaling the response using an exponential function $e^{\eta t}$ [23]. This technique is frequently employed by seismologists using integral transform methods and/or boundary elements [24].

The Boundary Element Method (BEM) has already been used to simulate the propagation of waves within, and between, fluid-filled boreholes [25]. These models are frequently applied in the seismic prospecting techniques known as acoustic logging and cross-hole surveying, used to determine the characteristics of the elastic medium in the vicinity of the boreholes. The Boundary Element Method (BEM) could be regarded as the best tool for modelling and analysing wave propagation in an unbounded medium, because it automatically satisfies the far field conditions. However, this method requires the prior knowledge of the Green's functions, which relate the field variables, as pressure and displacements, to the response to unit point loads applied somewhere in the medium. Different Greens' functions have been developed to allow complex frequencies to be used, and to obviate the need for discretizing surfaces, as with the half space model [26, 27].

In the case of an air filled enclosure, the problem is more complicated, given the low velocity of the sound wave propagation. FEM/BEM models have already been used in the study of room acoustics at low frequencies in cases where other numerical techniques are less well able to take the diffraction effects into account [19].

In our work, the pressure field produced by a point source inside a parallelepiped closed room was calculated using an analytical function, defined by means of the image model technique. The Allen and Berkley [2] model is followed, but in the frequency domain, and the impulse time responses are obtained by means of inverse Fourier transforms. The computations make use of complex frequencies, following the technique described earlier.

First, the analytical function is derived, assuming the existence of perfect reflecting surfaces. The resulting expression is theoretically interesting in itself, because it allows the sound pressure signal to be defined within an enclosed rectangular space, which is useful as a benchmark solution for numerical applications. Furthermore, it can be used as a Green's function in numerical techniques which employ integral transform methods and/or boundary elements. The next step involves a mathematically simplified manipulation of the analytical function to allow the use of absorption that varies in the space and frequency domains, which makes the model useful in comparison with other techniques, applied directly in the time domain. That is, each frequency response is computed taking into account the absorption of the various walls, which may be frequency dependent. The time results are then synthesised using inverse Fourier transform, modelling a Ricker pulse. The introduction of frequency dependence absorption would not be as straightforward to implement in a time domain formulation.

In the present paper, these final equations are used to obtain the reverberation times from the impulse responses using the Schroeder approach for different characteristic frequency excitation pulses.

The paper is organized as follows: first the analytical incident field generated by a harmonic point source is presented and the response solution (Green's function) is obtained for a rectangular closed space, assuming the existence of perfectly reflecting walls; then, simplified analytical functions are derived to incorporate wall absorption effects, and a brief section is included to illustrate the numerical procedure leading to time domain solutions. The main part of the article is devoted to simulating the propagation of sound generated by point sources inside an actual empty, enclosed space; reverberation times are computed and compared with those obtained using the simplified models devised by Sabine, Eyring, Millington, Fitzroy and Arau-Puchades, and, finally, the numerical results are compared with those provided by experimental measurements in situ.

2. Incident field generated by a point source

A harmonic point pressure load in the form $\delta(x-x_0)\delta(y-y_0)\delta(z-z_0)\mathrm{e}^{\mathrm{i}\omega t}$, acting at (x_0, y_0, z_0) in an infinite homogeneous acoustic space generates a pressure field defined by the equation:

$$p(\omega, x, y, z, t) = \frac{A\mathrm{e}^{\mathrm{i}\omega/c\left(ct-\sqrt{(x-x_0)^2+(y-y_0)^2+(z-z_0)^2}\right)}}{\sqrt{(x-x_0)^2+(y-y_0)^2+(z-z_0)^2}}. \quad (1)$$

In these expressions $\delta(x)$, $\delta(y)$ and $\delta(z)$ are Dirac-delta functions, ω is the frequency of the load, A is the wave amplitude, c is the propagation velocity of the pressure waves, and $\mathrm{i} = \sqrt{-1}$.

The insertion of perfectly reflecting barriers in the medium further modifies the acoustic pressure field. This effect can be obtained by using virtual sources placed so as to confirm the boundary conditions required (nil pressure flows). The first order image sources correspond to the first reflections originated by the reflecting walls, while high order image sources represent multiple reflections on the different walls. The number of virtual sources to be used in the calculations is defined so that the signal responses can be correctly computed in the time frame, which is determined by the frequency increment ($TD = 1/\Delta f$). Thus, the contributions of the virtual sources placed away from the receiver $c/\Delta f$ are not taken into account. This procedure does not introduce any type of error in the computed time impulse response within the time window defined, TD.

After some mathematical manipulations, the following expression is derived, defining the pressure field inside a closed rectangular room with dimensions d_1, d_2 and d_3, along the x-, y- and z-directions, respectively

$$\begin{aligned}\mathrm{p}(\omega, x, y, z) = A\Bigg\{ & \frac{\mathrm{e}^{-\mathrm{i}r_{000}\omega/c}}{r_{000}} + \sum_{n=0}^{NSV}\left[\sum_{j=1}^{4}\frac{\mathrm{e}^{-\mathrm{i}r_{0j0}\omega/c}}{r_{0j0}}\right] \\ & + \sum_{m=1}^{NSH}\sum_{i=1}^{4}\left\{\frac{\mathrm{e}^{-\mathrm{i}r_{i00}\omega/c}}{r_{i00}} + \sum_{n=0}^{NSV}\left[\sum_{j=1}^{4}\frac{\mathrm{e}^{-\mathrm{i}r_{ij0}\omega/c}}{r_{ij0}}\right]\right\}\Bigg\} \\ & + A\sum_{l=0}^{NSZ}\Bigg\{\sum_{k=1}^{4}\left\{\frac{\mathrm{e}^{-\mathrm{i}r_{00k}\omega/c}}{r_{00k}} + \sum_{n=0}^{NSV}\left[\sum_{j=1}^{4}\frac{\mathrm{e}^{-\mathrm{i}r_{0jk}\omega/c}}{r_{0jk}}\right]\right. \\ & \left. + \sum_{m=1}^{NSH}\sum_{i=1}^{4}\left\{\frac{\mathrm{e}^{-\mathrm{i}r_{i0k}\omega/c}}{r_{i0k}} + \sum_{n=0}^{NSV}\left[\sum_{j=1}^{4}\frac{\mathrm{e}^{-\mathrm{i}r_{ijk}\omega/c}}{r_{ijk}}\right]\right\}\right\}\Bigg\} \quad (2)\end{aligned}$$

where NSH, NSV, NSZ represents the number of sources used in the x-, y- and z-directions respectively, that are needed for the correct definition of the acoustic signal.The existence of an exponential factor $\mathrm{e}^{\mathrm{i}\omega t}$ in this equation is implicit. In this expression

$$\begin{aligned} r_{ijk} &= \sqrt{(\underline{x}_i)^2 + (\underline{y}_j)^2 + (\underline{z}_k)^2}, \\ \underline{x}_0 &= (x - x_0), \quad \underline{y}_0 = (y - y_0), \quad \underline{z}_0 = (z - z_0) \\ \underline{x}_1 &= (x + x_0 + 2d_1 m), \quad \underline{y}_1 = (y + y_0 + 2d_2 n), \\ \underline{z}_1 &= (z + z_0 + 2d_3 l), \\ \underline{x}_2 &= (x - 2d_1 - x_0 - 2d_1 m), \\ \underline{y}_2 &= (y - 2d_2 - y_0 - 2d_2 n), \\ \underline{z}_2 &= (z - 2d_3 - z_0 - 2d_3 l), \\ \underline{x}_3 &= (x + 2d_1 - x_0 + 2d_1 m), \\ \underline{y}_3 &= (y + 2d_2 - y_0 + 2d_2 n), \\ \underline{z}_3 &= (z + 2d_3 - z_0 + 2d_3 l), \\ \underline{x}_4 &= (x - 2d_1 + x_0 - 2d_1 m), \\ \underline{y}_4 &= (y - 2d_2 + y_0 - 2d_2 n), \\ \underline{z}_4 &= (z - 2d_3 + z_0 - 2d_3 l). \end{aligned}$$

3. Sound energy absorption

The above expression assumes the existence of perfectly reflecting walls. However, only part of the incident energy is reflected if the walls have some absorption characteristics. In the case of a plane incident sound wave, the relation between the absorbed energy and the incident energy can be given by $1 - |R^2|$, where R is the reflection coefficient, which is defined as the ratio of the reflected and incident sound pressure at the interface. The reflection coefficient for an incident sound plane wave falling obliquely on a plane interface is complex. The phase change of the reflected wave may vary from 0° to 180°. As an example, in a porous material layer, the phase angle of the reflection coefficient is close to zero when the surface admits high values of flow resistance at lower frequencies, whereas for a soft surface the reflection coefficient may undergo a 180° phase change when the flow resistance is low at higher frequencies [28]. Our work uses a point source, which can be seen as a sum of plane waves striking the wall from all

directions, making the solution of the problem complex. To simplify the solution, the impedance is assumed to be real, and the pressure reflection coefficient is computed as $R = \pm\sqrt{1-\alpha}$, where α is the fraction of the incident sound energy absorbed by the wall, ignoring the incidence angle.

In the numerical model described above, if the walls are not perfectly reflective, the response is obtained considering the application of pressure reflection coefficients R each time the pulse produced by a virtual source hits the wall. In the numerical examples presented here, two distinct situations are taken into account: either assuming the reflected pulse remains in-phase with the incident pulse ($R = \sqrt{1-\alpha}$), or assuming a $180°$ phase shift ($R = -\sqrt{1-\alpha}$). Since the computations are performed in the frequency domain, different reflection coefficients can be used for different frequencies. When constant reflection coefficients are used, they can be understood as global medium coefficients. Furthermore, different reflection coefficients can be ascribed to each wall, simulating a variety of absorptive materials. Equation (2) has been reformulated so as to accommodate the existence of different reflection coefficients

$$
\begin{aligned}
&\mathrm{p}(\omega,x,y,z) = \\
&\quad A\Bigg\{\frac{\mathrm{e}^{-\mathrm{i}r_{000}\omega/c}}{r_{000}} + \sum_{n=0}^{NSV}\sum_{j=1}^{4}\frac{\mathrm{e}^{-\mathrm{i}r_{0j0}\omega/c}R_{0j0}}{r_{0j0}} \\
&+ \sum_{m=1}^{NSH}\sum_{i=1}^{4}\left\{\frac{\mathrm{e}^{-\mathrm{i}r_{i00}\omega/c}R_{i00}}{r_{i00}} + \sum_{n=0}^{NSV}\sum_{j=1}^{4}\frac{\mathrm{e}^{-\mathrm{i}r_{ij0}\omega/c}R_{ij0}}{r_{ij0}}\right\} \\
&+ \sum_{l=0}^{NSZ}\sum_{k=1}^{4}\left\{\frac{\mathrm{e}^{-\mathrm{i}r_{00k}\omega/c}R_{00k}}{r_{00k}} + \sum_{n=0}^{NSV}\sum_{j=1}^{4}\frac{\mathrm{e}^{-\mathrm{i}r_{0jk}\omega/c}R_{0jk}}{r_{0jk}}\right\} \\
&+ \sum_{m=1}^{NSH}\sum_{i=1}^{4}\left\{\frac{\mathrm{e}^{-\mathrm{i}r_{i0k}\omega/c}R_{i0k}}{r_{i0k}}\right. \\
&\qquad\left.+ \sum_{n=0}^{NSV}\sum_{j=1}^{4}\frac{\mathrm{e}^{-\mathrm{i}r_{ijk}\omega/c}R_{ijk}}{r_{ijk}}\right\}\Bigg\}. \qquad (3)
\end{aligned}
$$

In this expression $R_{ijk} = R_{i00}R_{0j0}R_{00k}$, with

$$
\begin{aligned}
R_{000} &= 1.0, & R_{100} &= R_{le}(R_{le}R_{ri})^m, \\
R_{200} &= (R_{le}R_{ri})^{m+1}, & R_{300} &= (R_{le}R_{ri})^{m+1}, \\
R_{400} &= R_{ri}(R_{le}R_{ri})^m, & R_{010} &= R_{fl}(R_{fl}R_{ce})^n, \\
R_{020} &= (R_{fl}R_{ce})^{n+1}, & R_{030} &= (R_{fl}R_{ce})^{n+1}, \\
R_{040} &= R_{ce}(R_{fl}R_{ce})^n, & R_{001} &= R_{re}(R_{re}R_{fr})^l, \\
R_{002} &= (R_{re}R_{fr})^{l+1}, & R_{003} &= (R_{re}R_{fr})^{l+1}, \\
R_{004} &= R_{fr}(R_{re}R_{fr})^l,
\end{aligned}
$$

where R_{ce}, R_{fl}, R_{re}, R_{fr}, R_{ri} and R_{le} correspond to the reflection coefficients of the ceiling, floor, rear wall, front wall, right wall and left wall, respectively.

It must be noted that equation 3 only takes into account specular reflections, ignoring the diffuse component of the reflected energy.

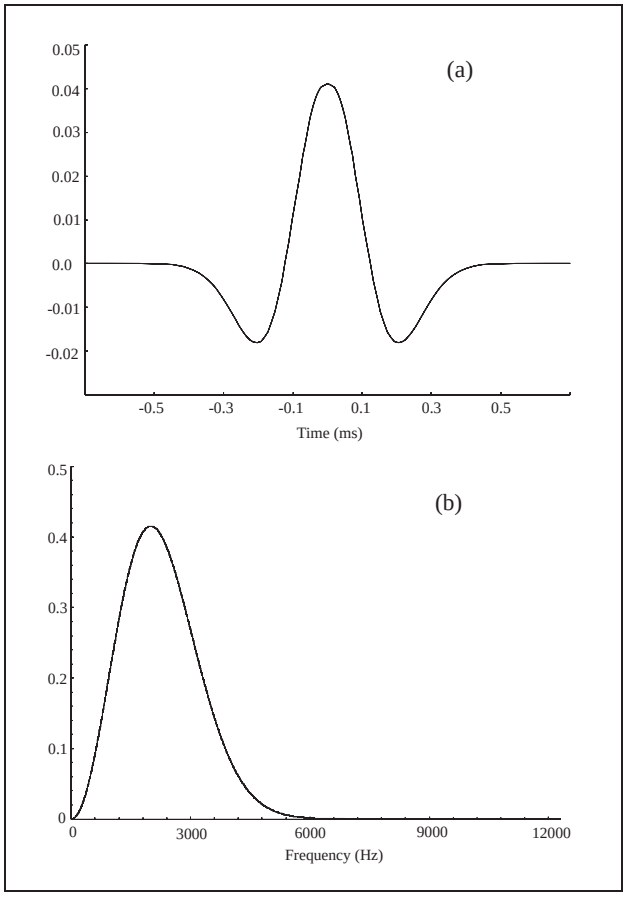

Figure 1. Ricker wavelet pulse: a) Time response; b) Spectrum.

4. Signals in the time domain

The computations are performed in the frequency domain, as mentioned above, with an increment $\Delta\omega$, and using complex frequencies to avoid a non-causal event occurring before the first true wave arrivals (i.e., aliasing phenomenon). The range of frequencies is defined by the type and duration of the pulse. If a Dirac delta pulse is used, the spectrum of frequencies will be infinite, which leads to an impracticable computation demand. Other types of pulse would be more appropriate. This explains why the type of pulse modelled will determine the computation cost of the problem. Here, we have chosen the Ricker pulse, because it decays rapidly in the time and frequency domains, which both requires less computational effort and makes interpretation of the time signals easier.

The pressure field in the time domain is computed by applying an inverse Fourier transform to the frequency response. The time-dependent excitation load function is defined as a Ricker wavelet pulse in the form

$$u(\tau) = A(1-2\tau^2)\,\mathrm{e}^{-\tau^2}, \qquad (4)$$

where A is the amplitude, $\tau = (t-t_s)/t_0$, t refers to time, t_s is the time at which the maximum occurs, while $\pi\, t_0$ is the characteristic period of the wavelet.

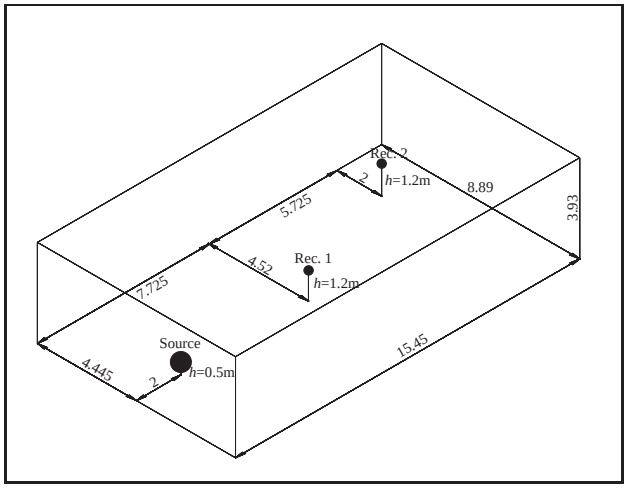

Figure 2. Geometry of the model.

Its Fourier transform is given by

$$U(\omega) = A\left[2\sqrt{\pi}t_0 \mathrm{e}^{-\mathrm{i}\omega t_s}\right] \Omega^2 \, \mathrm{e}^{-\Omega^2}, \qquad (5)$$

in which $\Omega = \omega t_0/2$.

The multiplication of this source function by the transfer function, defined by the previous computations in the frequency domain, allows the response of a Ricker pulse excitation to be found. The range of frequencies goes up to three times the characteristic frequency of the pulse. The contribution to the response behind this range of frequencies is close to zero. Figure 1 shows the source signature in the time domain and its frequency spectrum, obtained for a pulse with a characteristic frequency of 2000 Hz.

5. Applications

All the applications in this work use a rectangular closed room with dimensions $d_1 = 8.89\,\mathrm{m}$, $d_2 = 3.93\,\mathrm{m}$ and $d_3 = 15.45\,\mathrm{m}$. This was an empty room in the University of Coimbra - Portugal, made of solid walls. At present, the room serves as an excellent laboratory, useful for comparing numerical results with those provided by in situ measurements. The acoustic behavior of this room is first studied using the numerical model described above. Then, the reverberation times obtained are compared with those provided by the simplified formulas. Different scenarios are simulated: that ascribed to the walls' surfaces, absorption (which varies from low to high values, and for even and uneven distributions), in an attempt to understand the behavior of our model. Finally, the in situ measurements are compared with numerical computations.

5.1. Numerical examples

The numerical model assumes that the acoustic space is illuminated by a point pressure source placed at O ($x_0 = 4.445\,\mathrm{m}$; $y_0 = 0.5\,\mathrm{m}$; $z_0 = 2.0\,\mathrm{m}$). The waves generated propagate in all directions with a velocity of 340 m/s. The three-dimensional pressure wavefield generated is computed using the analytical function defined in equation (3),

Table I. Absorption coefficients.

	Ceiling	Floor	Rear	Front	Right	Left
Case 1	0.05	0.05	0.05	0.05	0.05	0.05
Case 2	0.1	0.1	0.1	0.1	0.1	0.1
Case 3	0.3	0.3	0.3	0.3	0.3	0.3
Case 4	0.5	0.5	0.5	0.5	0.5	0.5
Case 5	0.7	0.7	0.7	0.7	0.7	0.7
Case 6	0.05	0.05	0.05	0.05	0.7	0.05
Case 7	0.05	0.05	0.7	0.05	0.05	0.05
Case 8	0.7	0.05	0.05	0.05	0.05	0.05

Table II. Range of computed frequencies.

	Δf (Hz)	$TD(s)$	f_0	NF	f_{max}
Case 1	0.3	3.33	0.3	65536	19660.8
Case 2	0.375	2.67	0.375	32768	12288.0
Case 3	0.75	1.33	0.75	16384	12288.0
Case 4	0.75	1.33	0.75	16384	12288.0
Case 5	0.75	1.33	0.75	16384	12288.0
Case 6	0.375	2.67	0.375	32768	12288.0
Case 7	0.375	2.67	0.375	32768	12288.0
Case 8	0.375	2.67	0.375	32768	12288.0

at two receivers placed at ($x = 4.445\,\mathrm{m}$; $y = 1.20\,\mathrm{m}$; $z = 7.725\,\mathrm{m}$) and ($x = 2.00\,\mathrm{m}$; $y = 1.20\,\mathrm{m}$; $z = 13.45\,\mathrm{m}$), respectively, as illustrated in Figure 2.

Eight simulations are performed, ascribing different absorption coefficients for the walls, ceiling and floor as listed in Table I.

Constant absorption coefficients for all walls are attributed in cases 1 to 5. Within these simulations, the absorption coefficients range from low values, $\alpha = 0.05$, to higher values, $\alpha = 0.7$, as we move from case 1 to case 5. Cases 6 to 8 are similar to case 1, but the absorption coefficient of the right, rear wall and ceiling has been changed to $\alpha = 0.7$. The calculations are performed in the frequency domain, in the range $[f_0, f_{max}]$, with a frequency increment of Δf (Hz), allowing analysis in the time domain to be defined up to TD, as listed in Table II. An inverse Fourier transform is applied to the response to obtain the signal in the time domain, using Ricker pulses with different characteristic frequencies: 125 Hz, 250 Hz, 500 Hz, 1000 Hz, 2000 Hz, 4000 Hz. As mentioned above, the numerical calculations have been performed for two situations: assuming the reflected pulse to remain in-phase with the incident pulse ($R = \sqrt{1-\alpha}$), or assuming a 180° phase shift ($R = -\sqrt{1-\alpha}$).

The estimation of the reverberation time for each response is obtained by integrating the energy of the signal using the Schroeder approach,

$$S(t) = \int_0^{TD} p^2(\tau)\,\mathrm{d}\tau - \int_0^t p^2(\tau)\,\mathrm{d}\tau, \qquad (6)$$

where p is the pressure in the time domain and $S(0)$ is the total energy over the total time range, TD. The results

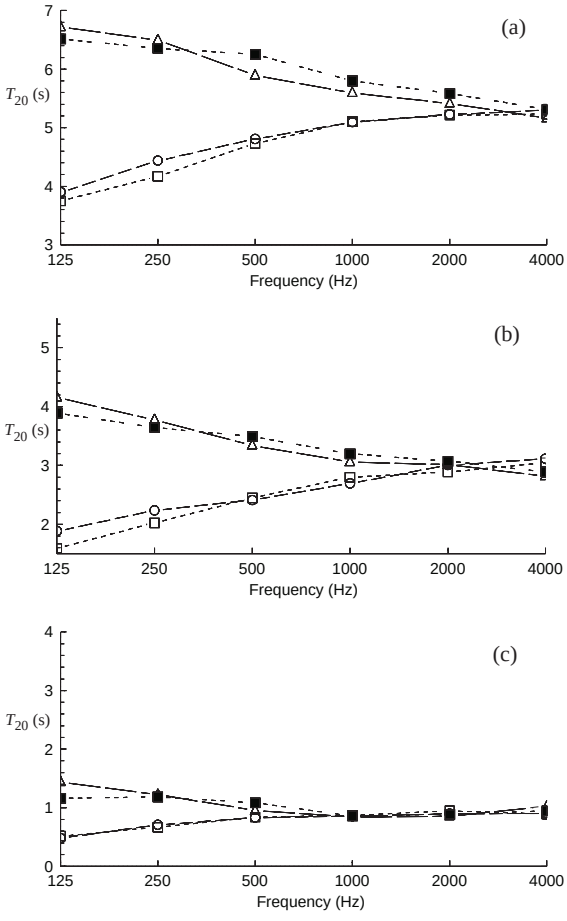

	Sabine	Eyring	Millington	Titzroy	Arau-Puch.
(a)	3.7645	3.6696			3.6704
(b)	1.8823	1.7865			
(c)	0.6274	0.5277			
(d)	0.3765	0.2716			
(e)	0.2689	0.1563			

Figure 4. Reverberation times provided by the numerical model and by the simplified formulas: a) Case 1, absorption = 0.05; b) Case 2, absorption = 0.1; c) Case 3, absorption = 0.3; d) Case 4, absorption = 0.5; e) Case 5, absorption = 0.7.

have been plotted against $s(0)$ on a dB scale. The results obtained are compared with those given by applying the simplified models, given in the Appendix.

Next, the methodology described above is demonstrated in the calculation of the reverberation time at receiver 1, when the case 2 absorption coefficients are ascribed to the walls, floor and ceiling. Figure 3a presents the evolution of the pressure over time, generated by a source pulse with a characteristic frequency of 500 Hz. Figure 3b gives the results of the energy integration, using the procedure described above (equation 6). The resulting plot shows a smooth reduction in the energy level as time advances. The reverberation times are computed as indicated in ISO 3382 [29].

Figure 4 summarizes the results obtained at receivers 1 and 2, when the numerical model is applied to cases 1 to 5, for both the in-phase and $180°$ phase reflection coefficients. The amplitude range of the vertical axis (reverberation times) is kept constant to permit easier interpretation of the results. The reverberation times calculated by the simplified models of Fitzroy, Millington, Eyring, Sabine and Arau-Puchades are also listed below these plots. These models provide reverberation times for harmonic sources but do not take into account the position of the receivers. The numerical results displayed in Figure 4 show that the reverberation times depend both on the characteristic frequency of the pulse excited and on the position of the receivers, even when the material properties of the walls remain constant for the whole frequency domain of the time signal. This behavior is even more pronounced if the absorption of the room is reduced, when the reverberation time varies significantly with the frequency of the excitation source, and the position of the receivers assumes more importance.

The results also confirm that when the reflection coefficients are assumed to change phase each time a pulse hits a wall surface, the reverberation times are smaller at lower excitation frequencies than those obtained when no phase change occurs. At higher frequencies, the reverberation times provided by the two models are closer to each other. These results can be explained by the fact that the time signals are a sequence of pulses that correspond to the incident pulse, and a train of pulses, which have been successively reflected on the wall surfaces during the time period. At lower frequencies, two successive pulses may not arrive at the receivers with a sufficient time lapse to avoid their overlapping. Thus, the resulting pulse is smaller when the phase of the two pulses evidences a phase change of $180°$.

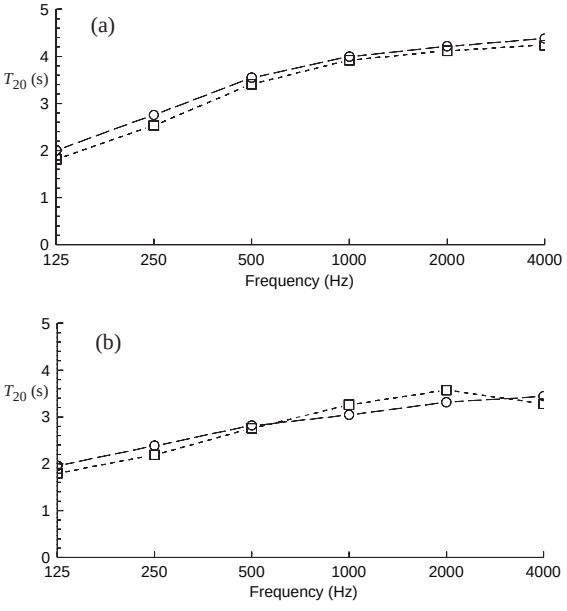

	Sabine	Eyring	Millington	Titzroy	Arau-Puch.
(a)	1.3975	1.3011	0.9342	3.2118	2.0607
(b)	1.9064	1.8107	1.3668	3.3062	2.6331
(c)	0.7791	0.6807	0.4814	2.6341	0.9945

Figure 5. Reverberation times provided by the numerical model and by the simplified formulas: a) Case 6; b) Case 7; c) Case 8.

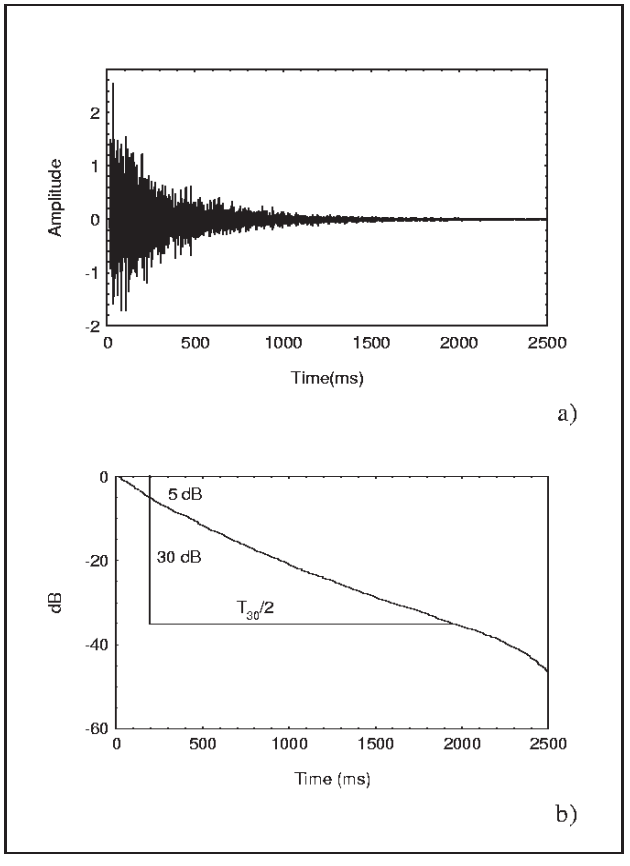

Figure 3. Responses at receiver 1 (case 2): a) time pressure response; b) energy integration plot.

Meanwhile, at higher frequencies the pulses are narrower in the time domain, and the overlapping phenomenon may not occur. Two successive reflected pulses may have a phase difference, but their amplitude may remain similar to that obtained when no change of phase occurs. So, at higher frequencies the energy of the signals at a specific receiver tends to exhibit similar energy decay, leading to similar reverberation times.

Analysis of the different simplified formulae results reveals that they tend to approximate as the absorption coefficients diminish. When the formulas' results are compared with those given by the numerical computations, a very good agreement is found at low frequencies (125 Hz) for the model assuming the existence of phase change. For higher absorption coefficients (Case 5), the numerical model approaches Sabine's model at lower frequencies. The numerical results depart from the simplified formulae calculations as the absorption of the room decreases, particularly for higher frequencies. The model which assumes no phase change does not appear to be suitable for simulating this room.

Figure 5 illustrates the responses obtained for an uneven distribution of surface absorption, Cases 6 to 8. Here, the Case 1 absorption coefficients, ascribed to the walls, floor and ceiling, are changed to accommodate, first, an absorption coefficient of the right wall, $\alpha = 0.7$ (Case 6), then an absorption coefficient of the rear wall, $\alpha = 0.7$ (Case 7), and finally an absorption coefficient, $\alpha = 0.7$, for the ceiling. The simplified models give markedly different predictions. Of the various models, Fitzroy's model predicts higher reverberation times. The numerical computations reveal similar features to the ones registered above. Only the results obtained by the model using phase change are displayed. At lower frequencies, the results approach those given by Sabine's model for Cases 7 and 8, while the results obtained for Case 6 fall within the range of results provided by the simplified formulas. As Dance *et al.* [17]

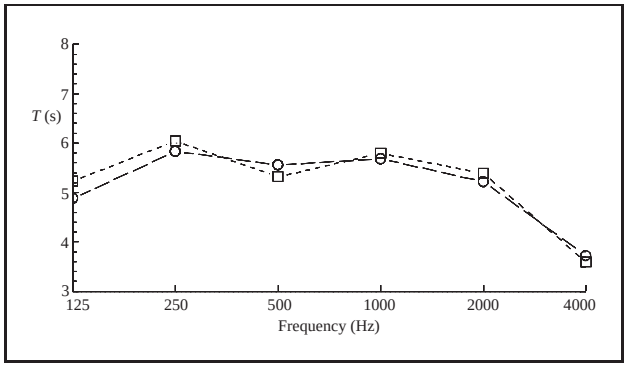

Figure 6. Reverberation times measured.

noted, the Millington formula predicts reverberation times which differ from both the numerical model and from the other simplified formulas.

At higher frequencies, our results agree with those provided by Fitzroy's model for Case 7, while higher reverberation times are computed numerically for Cases 6 and 8. Furthermore, our results indicate that the position of the receivers is less important when the ceiling has higher absorption, while the position of the receivers is more relevant when higher absorption is ascribed to the rear wall.

5.2. Experimental results

As the problem is quite complex, in situ tests are frequently used to measure reverberation times. Nowadays, the methods for measuring them are regulated by international standards such as the ISO 3382 [29].

The experimental work entailed measuring reverberation times in situ. The data acquisition was provided by a *Symphonie* system unit, from *01dB MVI Technologies Group*, directly onto the computer hard disk via a *PC card* interface, using building acoustics measurement and processing software, *dBBATI32*. The test signal used was a MLS (Maximum Length Sequence) noise signal. The response duration was set to 5.2 s, and the average number was set to 8 to diminish the effect of background noise. Thus, measurements were performed individually at each receiver position for 41.6 s. Omnidirectional microphones were used, connected directly to the *Symphonie* system unit.

The sound source (Brüel&Kjær type 4224) employed was a dual-concentric, single way loudspeaker mounted in a rectangular box, placed at position O. As this sound is not an omnidirectional source, different measurements were performed placing the source in different directions. The final reverberation times, illustrated in Figure 6, were computed taking the average of these measurements.

5.3. Comparison with numerical simulations

Synthetic impulse responses were computed using the numerical model described above, taking the absorption coefficients predicted by the inverse use of Sabine's model (see Table III), applied to the values measured.

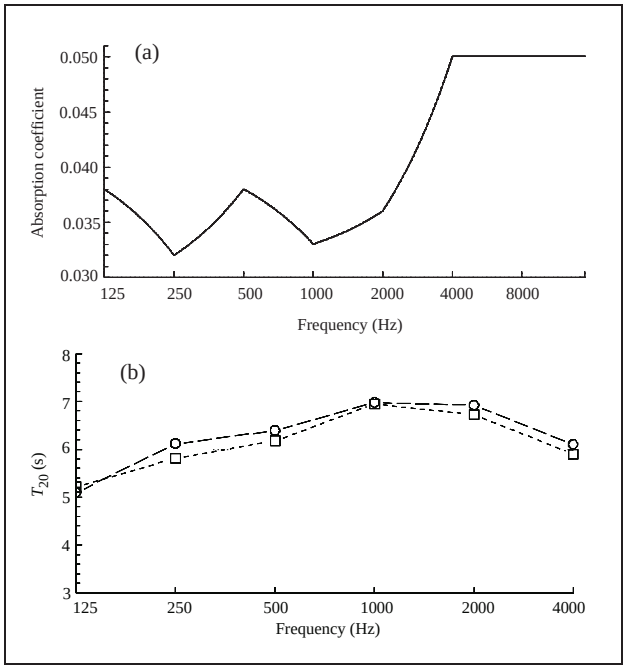

Figure 7. Numerical model results a) absorption coefficient frequency dependence used; b) Reverberation times computed.

Table III. Absorption coefficients defined by the inverse use of Sabine's mode.

f (Hz)	125	250	500	1000	2000	4000
α	0.038	0.032	0.038	0.033	0.036	0.05

The computations were performed in the frequency range from 0.23 Hz to 15073.28 Hz, with a frequency increment of 0.23 Hz, defining a time window for the analysis of 4.35 s. The absorption coefficient dependence in the full frequency domain, was then held to be defined by connecting the values of the absorption coefficients defined in Table III with straight lines. Figure 7a shows the absorption curve defined, using a logarithmic scale.

After computing the impulse responses, the reverberation times were then calculated using the procedure described above, and assuming a phase shift (see Figure 7b). These results agree with those measured in situ at lower frequencies, while they diverge for higher frequencies. Some of these discrepancies may be attributed to the existence of diffuse surface reflections, not taken into account by our numerical model. Hodgson [8, 10], when comparing the sound decay predicted by a ray tracing technique with experimental measurements, concluded that the importance of the diffuse effects grows when disproportionate rooms (with one dimension very different from the others) are used and as the frequency increases. Furthermore, our model does not take air absorption into account.

Precise knowledge of the material's absorption and diffusivity properties would allow the proposed model to be improved if a diffuse field absorption coefficient were to take into account both the diffuse and specular reflec-

tions. These material absorption and diffusivity properties should be based on in situ measurements for both absorption and diffusivity, as a number of authors have proposed [30, 31].

6. Conclusions

This work has described analytical solutions for defining the pressure response inside an empty parallelepiped closed space subjected to a harmonic point source, using an image source technique in the frequency domain. The model provided synthetic responses, which were then used to compute reverberation times, adopting the Schroeder approach.

The results computed for a large room have been compared with those provided by the simplified models of Sabine, Eyring, Millington, Fitzroy and Arau-Puchades, which are obtained for harmonic pressure sources and do not take into account the position of the receivers. Furthermore, these simplified models predict constant reverberation times for different frequency harmonic sources if the absorption coefficients of the surfaces are kept constant. The numerical results confirm that the reverberation time varies significantly with both the frequency of the excitation source and the position of the receivers.

The simplified formulas' results tend to approximate for lower absorption coefficients. The results provided by our model, using a $180°$ phase change, agree with the simplified formulas at lower frequencies, while they diverge for higher frequencies. As the absorption increases, however, the numerical results approach those given by Sabine's model, even for high frequencies.

In addition, measurements inside an empty room with concrete walls were then taken using an appropriate chain of measurement. The reverberation times were then compared with those yielded by the numerical model, using absorption coefficients predicted by the inverse use of Sabine's model on the measured results. Good agreement was found at lower frequencies, while the numerical results diverged as the frequency of excitation increased. These differences may be the result of the presence of diffuse effects not taken into account in the numerical model but which are more important for higher frequencies.

Appendix

Reverberation time models:

Sabine model [32],

$$RT_{60} = 0.1625 \frac{V}{\sum_{i=1}^{N} S_i \alpha_i}; \qquad \text{(A1)}$$

Eyring model [33],

$$RT_{60} = 0.1625 \frac{V}{-S \ln(1-\alpha_a)}; \qquad \text{(A2)}$$

Millington model [34],

$$RT_{60} = 0.1625 \frac{V}{-\sum_{i=1}^{N} \left(S_i \ln(1-\alpha_i)\right)}; \qquad \text{(A3)}$$

Fitzroy model [35],

$$RT_{60} = \frac{0.1625V}{S^2} \left[\frac{2d_1 d_2}{-\ln(1-\alpha_{XY})} + \frac{2d_1 d_3}{-\ln(1-\alpha_{XZ})} + \frac{2d_2 d_3}{-\ln(1-\alpha_{YZ})} \right], \qquad \text{(A4)}$$

Arau-Puchades model [36],

$$RT_{60} = \left[\frac{6}{\bar{a}_x N \log e} \right]^{(2d_2 d_3)/S} \left[\frac{6}{\bar{a}_y N \log e} \right]^{(2d_1 d_3)/S} \cdot \left[\frac{6}{\bar{a}_z N \log e} \right]^{(2d_1 d_3)/S}, \qquad \text{(A5)}$$

where RT_{60} is the time required for an interrupted steady-state signal in a space to decay 60 dB, V is the volume of the room in cubic meters, N is the number of different materials, S_i is the area of the material i, α_i is the absorption coefficient of the material i,

$$\alpha_a = \sum_{i=1}^{N} S_i \alpha_i \Big/ \sum_{i=1}^{N} S_i \,,$$

α_{ij} is the average absorption coefficient of the wall ij.

$$S = 2d_1 d_2 + 2d_1 d_3 + 2d_2 d_3,$$

$\bar{a}_x$, $\bar{a}_y$ and $\bar{a}_z$ are the mean decay rate absorption coefficients in the direction x, y and z, respectively, $N = c/l_m$ with l_m frequently assumed to be $4V/S$.

References

[1] M. Vorländer: Simulation of the transient and steady-state sound propagation in rooms using a new combined ray-tracing/image-source algorithm. J. Acoust. Soc. Am. **86** (1989) 172–178.

[2] J. B. Allen, D. A. Berkley: Image method for efficiently simulating small room acoustics. J. Acoust. Soc. Am. **65** (1979) 943–950.

[3] R. N. S. Hammad: Simulation of noise distribution in rectangular rooms by means of computer modeling techniques. Applied Acoustics **24** (1988) 211–228.

[4] H. Lee, B. Lee: An efficient algorithm for the image model technique. Applied Acoustics **24** (1988) 87–115.

[5] A. Kulowski: Error investigation for the ray tracing technique. Applied Acoustics **15** (1982) 263–274.

[6] U. Stephenson: Comparison of the mirror image source method and the sound particle simulation method. Applied Acoustics **29** (1990) 35–72.

[7] A. Kulowski: Algorithmic representation of the ray tracing technique. Applied Acoustics **18** (1985) 446–469.

[8] M. Hodgson: Evidence of diffuse surface reflections in rooms. J. Acoust. Soc. Am. **89** (1991) 765–771.

[9] H. Kuttruff: Room acoustics. Applied Science, London, 1976.
[10] M. Hodgson: On the prediction of sound fields in large empty rooms. J. Acoust. Soc. Am. **84** (1988) 253–261.
[11] B.-I. Dalenbäck: Room acoustic prediction based on a unified treatment of diffuse and specular reflection. J. Acoust. Soc. Am. **100** (1996) 899–909.
[12] B. M. Gibbs, D. K. Jones: A simple image method for calculating the distribution of sound pressure levels within an enclosure. Acustica **26** (1972) 24–32.
[13] J. Borish: Extension of the image model to arbitrary polyhedra. J. Acoust. Soc. Am. **75** (1984) 1828–1836.
[14] S. Dance, J. Roberts, B. Shield: Computer prediction of insertion loss due to a single barrier in a non-diffuse empty enclosed space. Journal of Building Acoustics **2** (1994) 125–136.
[15] A. Farina: RAMSETE - A new pyramid tracer for medium and large scale acoustic problems. Proc. Euronoise 95, 1995, 55–60.
[16] S. Dance, B. Shield: The complete image-source method for the prediction of sound distribution in non-diffuse enclosed spaces. Journal of Sound and Vibration **201** (1997) 473–489.
[17] S. M. Dance, B. M. Shield: Modelling of sound fields in enclosed spaces with absorbent room surfaces. part ii. absorptive panels. Applied Acoustics **61** (2000) 373–384.
[18] I. Bork: A comparison of room simulation software - the 2nd round robin on room acoustical computer simulation. Acustica **86** (2000) 943–956.
[19] O. Schmitz, G. Bartsch: Kombinierte Simulationsverfahren für die Raumakustik basierend auf FEM/BEM und geometrischen Modellen. Fortschritte der Akustik DAGA '98, Zurich, 1998, 708–709.
[20] G. D. Manolis, D. E. Beskos: Boundary element methods in elastodynamics. Unwin Hyman (sold to Chapman and Hall), London, 1988.
[21] A. J. B. Tadeu, J. M. P. António: Use of constant, linear and quadratic boundary elements in 3D wave diffraction analysis. EABE - Engineering Analysis with Boundary Elements **24** (2000) 131–144.
[22] M. Bouchon, K. Aki: Discrete wave-number representation of seismic-source wave field. Bull. Seism. Soc. Am. **67** (1977) 259–277.
[23] E. Kausel, J. M. Roesset: Frequency domain analysis of undamped systems. Journal of Engineering Mechanics ASCE **118** (1992) 721–734.
[24] D. P. Schmitt, M. Bouchon: Full-wave acoustic logging: synthetic microseismograms and frequency-wavenumber analysis. Geophysics **50** (1985) 1756–1778.
[25] W. Dong, M. Bouchon, M. N. Toksoz: Borehole seismic-source radiation in layered isotropic and anisotropic media: Boundary element modeling. Geophysics **60** (1995) 735–747.
[26] A. Tadeu, E. Kausel: Green's functions for two-and-a-half dimensional elastodynamic problems. Journal of Engineering Mechanics (ASCE) **126** (2000) 1093–1097.
[27] A. Tadeu, J. Antonio, L. Godinho: Green's function for two-and-a-half dimensional elastodynamic problems in a half-space. Computational Mechanics Journal **27** (2001) 484–491.
[28] L. L. Beranek: Noise and vibration control. Institute of Noise Control Engineering, Washington DC, 1988.
[29] ISO 3382 - acoustics: measurement of reverberation time of rooms with reference to other acoustical parameters. 1997.
[30] U. Wilms, R. Heinz: In situ Messung komplexer Reflexionsfaktoren von Wandflächen. Acustica **75** (1991) 28–39.
[31] L. Beranek, T. Hidaka: Sound absorption in concert halls by seats, occupied, and unoccupied, and by the hall's interior surfaces. J. Acoust. Soc. Am. **104** (1998) 3169–3177.
[32] W. C. Sabine: Collected papers in acoustics. Cambridge: Harvard University Press, 1992.
[33] C. F. Eyring: Reverberation time in dead rooms. Journal of the Acoustical Society of America **1** (1930) 217–241.
[34] G. Millington: A modified formula for reverberation. Journal of the Acoustical Society of America **4** (1932) 69–82.
[35] D. Fitzroy: Reverberation formula which seems to be more accurate with nonuniform distribution of absorption. Journal of Acoustical Society of America **31** (1959) 893–897.
[36] H. Arau-Puchades: An improved reverberation formula. Acustica **65** (1988) 163–180.